

# Supplementary Materials to: Mixed diffusive/martensitic character of the pressure-induced $\beta \leftrightarrow \gamma$ transformation in tin

Robin Fréville<sup>1,2</sup>, Agnès Dewaele<sup>3,4</sup>, Charles Pépin<sup>3,4</sup>, Nicolas Bruzy<sup>3,4</sup>, Florent Occelli<sup>3,4</sup>,  
Matteo Levantino<sup>2</sup>, Nicolas Guignot<sup>5</sup>

<sup>1</sup> Karlsruhe Institute of Technology, Institute for Applied Materials, P.O. Box 3640, 76021  
Karlsruhe, Germany

<sup>2</sup> European Synchrotron Radiation Facility, 71 Avenue des Martyrs, CS 40220, 38043 Grenoble,  
France

<sup>3</sup> CEA, DAM, DIF, F-91297 Arpajon, France

<sup>4</sup> Université Paris-Saclay, CEA, Laboratoire Matière en Conditions Extrêmes, 91680  
Bruyères-le-Châtel, France

<sup>5</sup> Synchrotron Soleil, BP 48, 91192 Gif-sur-Yvette Cedex, France

1 **S.A. TWINNING ELEMENTS**

2 Due to the reduced number of symmetries of  $\beta$ -Sn and  $\gamma$ -Sn compared to, e.g., cubic  
3 phases, twinning is likely to be frequently activated in these phases.

4 All twinning systems discussed in the text are reported in Table S1. For  $\beta$ -Sn, they have  
5 been observed directly [16, 48–50]. To our knowledge,  $\gamma$ -Sn being a high pressure phase, its  
6 twinning elements have not been measured. Indium has a crystal structure identical to  $\gamma$ -Sn:  
7 bct I4/mmm with  $a = 4.60 \text{ \AA}$  and  $c = 4.95 \text{ \AA}$  under ambient conditions;  $(101)_\gamma$  twinning is  
8 described for this metal [50]. It can be seen as an exchange between  $\vec{a}$  and  $\vec{c}$  axes, producing  
9 a rotation of  $85^\circ$  around  $\vec{b}$  axis. Another twinning system is described for bcc crystals, noted  
10 here  $(112)_\gamma$ ; such deformation is also possible for bct crystals as noted in [16] and has been  
11 reported for bct steel [51].

Phase	Structure	K1	$\eta_1$	K2	$\eta_2$	P	Ref.	Misorientation	Noted
$\beta$ -Sn	dbct I41/amd	(-301)	[103]	(101)	[-101]	(010)	[16, 48, 49]	$62.8^\circ$ around (010)	$(301)_\beta$
$\beta$ -Sn	dbct I41/amd	(101)	[-101]	(-301)	[103]	(010)	[16, 48–50]	$57.2^\circ$ around (010)	$(101)_\beta$
$\gamma$ -Sn	Bct I4/mmm	(101)	[10-1]	(-101)	[101]	(1-10)	[16, 50]	$85^\circ$ around (010)	$(101)_\gamma$
$\gamma$ -Sn	Bct I4/mmm	(112)	[-1-11]	(11-2)	[111]	(1-10)	[16, 51]	$68^\circ$ around (1-10)	$(112)_\gamma$

TABLE S1: Possible twinning systems for  $\beta$ -Sn and  $\gamma$ -Sn. The twinning elements are as defined in Ref. [16]: K1 and K2 twinning and reciprocal planes;  $\eta_1$  and  $\eta_2$  twinning and reciprocal directions. P is the plane of shear.

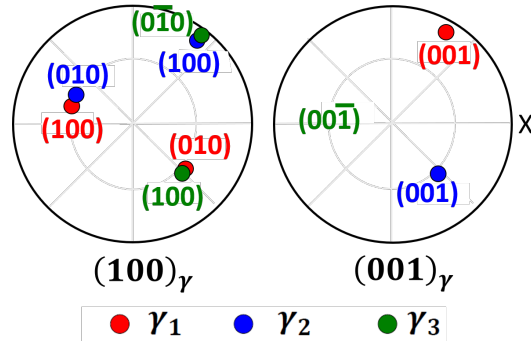


FIG. S1: Pole figure showing a clear twinning relationship between the three  $\gamma$  grains formed during Cycle 1, run 1. X is the compression axis.

12 **S.B. CONDITIONS OF THE TRANSFORMATION AND EQUATION OF STATE**

13 The  $\beta$ -Sn  $\leftrightarrow$   $\gamma$ -Sn transition pressures for all cycles of Runs 1 and 2 are reported in  
 14 Table S2. For both runs, no  $\beta$ -Sn- $\gamma$ -Sn coexistence domain was observed, with pressure  
 15 steps of  $\sim 0.2$  GPa. This differs from one previous report where a  $\beta$ -Sn polycrystal was  
 16 compressed: a  $\beta$ -Sn- $\gamma$ -Sn coexistence domain was observed between 10.8 GPa and 15.6 GPa  
 17 at 300 K [10]. Table S2 shows that transition pressures are all consistent for the direct  
 18  $\beta$ -Sn  $\rightarrow$   $\gamma$ -Sn transition, within  $\pm 0.2$  GPa. Interestingly, more scatter is observed for the  
 19 reversion ( $\pm 0.8$  GPa).

Run, cycle	$P_{\beta \rightarrow \gamma}$ (GPa)	$P_{\gamma \rightarrow \beta}$ (GPa)	Ref.
Run 1, 1	$10.7 \pm 0.2$	$8.8 \pm 0.1$	TW
Run 1, 2	$11.0 \pm 0.1$	$8.7 \pm 0.1$	TW
Run 2, 1	$10.9 \pm 0.1$	$9.2 \pm 0.3$	TW
Run 2, 2	$11.0 \pm 0.3$	$9.8 \pm 0.3$	TW
Run 2, 3	$10.9 \pm 0.6$	$9.7 \pm 0.6$	TW
Run 2, 4	$10.9 \pm 0.2$	$10.2 \pm 0.3$	TW
Run 2, 5	$11.1 \pm 0.4$		TW
	$10.8 \pm 4.8$		[10]

TABLE S2: Pressures measured for the  $\beta$ -Sn $\leftrightarrow$  $\gamma$ -Sn transitions, for the grains followed in this study.  $\pm$  indicate maximum coexistence domains. Data from ref. [10] (static hydrostatic loading) are included for comparison. TW: this work.

20 The  $P$ - $V$  points collected during the two runs (compression and decompression) agree  
 21 with the literature [10] as shown in the EOS displayed in Fig. S2. No drastic change in  
 22  $c_{\beta}/a_{\beta}$  or  $c_{\gamma}/a_{\gamma}$  was measured near the transitions. Here,  $c_{\beta}/a_{\beta}$  has a roughly constant value  
 23 of 0.543;  $c_{\gamma}/a_{\gamma} = 0.912$  at 11 GPa and increases with pressure as described in [10].

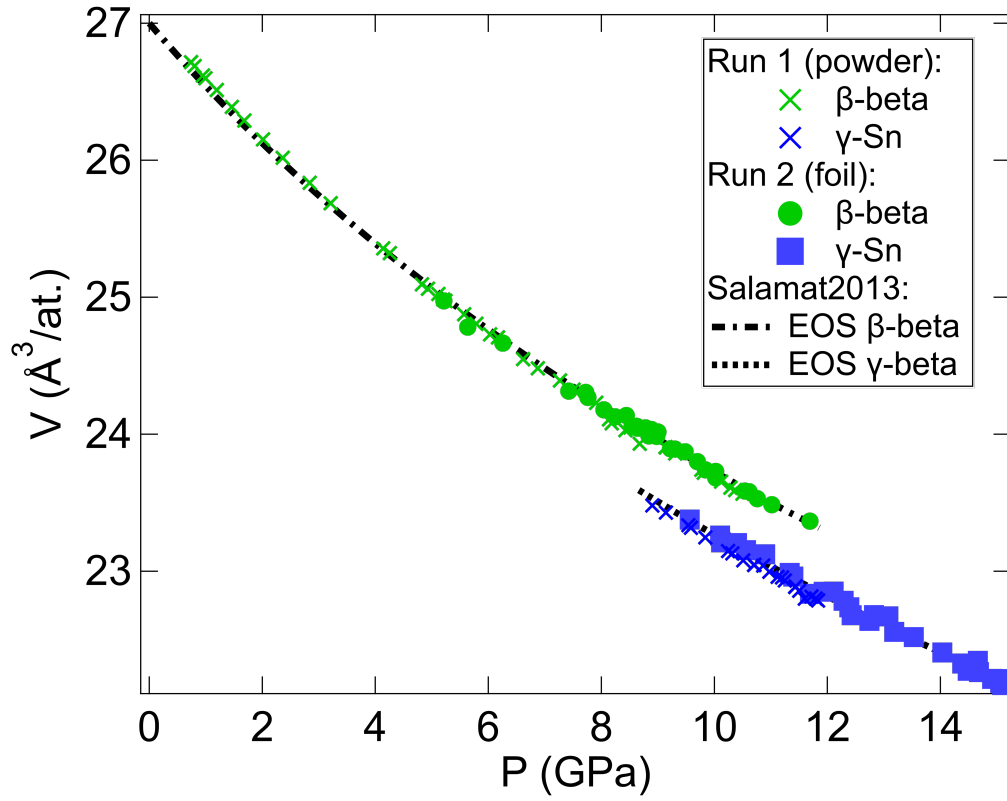


FIG. S2: Volume of  $\beta$ -Sn and  $\gamma$ -Sn measured on multiple compression/decompression cycles. EOS from Salamat et al. [10] are also plotted as dashed lines for comparison.

24 **S.C. CRYSTAL QUALITY EVOLUTION WITH CYCLES**

25 Fig. S3 shows an enlarged part of XRD images around one XRD peak during the exper-  
 26 iment. It shows that the starting grain in Run 1 has a higher mosaicity than in Run 2, and  
 27 the crystal healing after  $\gamma$ -Sn  $\rightarrow$   $\beta$ -Sn transition in Run 2.

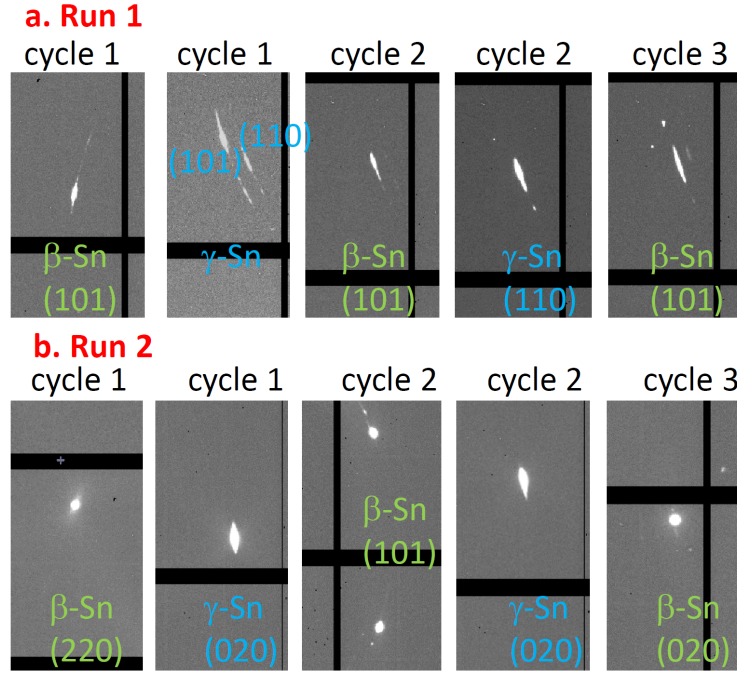


FIG. S3: Enlarged part of XRD images collected during Run 1 (a) and Run 2 (b). The starting grain in Run 1 had a high mosaicity ( $\sim 3^\circ$  FWHM extension in azimuthal angle  $\chi$ ), which further increased during the experiment ( $\sim 4^\circ$  FWHM in  $\chi$  in cycle 3). For Run 2, an  $\sim 1^\circ/\sim 3.5^\circ$  FWHM extension is measured in  $\beta$ -Sn/ $\gamma$ -Sn for cycles 1-3.

28 **S.D. EULER ANGLES AND ADDITIONAL POLE FIGURES**

29 Table S3 reports Euler angles determined during our static experiment using a Bunge  
30 convention.

Run 1						Run 2									
$\phi_1$	$\Phi$	$\phi_2$	$\phi_1$	$\Phi$	$\phi_2$	$\phi_1$	$\Phi$	$\phi_2$	$\phi_1$	$\Phi$	$\phi_2$				
$\beta_1$	212.0°	77.5°	272.9°	$\gamma_1$	-134.2°	83.6°	-144.5°	$\beta_A$	-82.0°	84.4°	23.6°	$\gamma_A$	85.1°	20.8°	-9.0°
$\beta_2$	-168.2°	80.4°	-257.4°	$\gamma_2$	-49.0°	50.9°	81.5°	$\beta_B$	7.2°	269.9°	229.1°	$\gamma_B$	19.5°	304.3°	66.0°
$\beta_2^*$	-111.8°	9.9°	18.6°	$\gamma_3$	-58.7°	143.1°	-185.1°	$\beta_C$	-3.0°	170.9°	176.9°	$\gamma_C$	15.2°	290.4°	129.3°
				$\gamma_4$	306.5°	52.4°	83.0°					$\gamma_D$	-66.1°	231.3°	-67.9°
				$\gamma_5$	111.3°	68.3°	294.3°					$\gamma_{2A}$	64.2°	264.0°	-13.9°
				$\gamma_6$	91.7°	132.5°	289.7°					$\gamma_{2B}$	-65.0°	70.7°	245.2°
				$\gamma_5^*$	121.7°	71.4°	65.5°					$\gamma_E$	26.8°	97.8°	14.8°
												$\gamma_F$	-31.8°	247.9°	156.3°
												$\gamma_G$	28.9°	63.6°	61.8°
												$\gamma_H$	-29.3°	91.9°	74.8°

TABLE S3: Euler angles determined by XRD in this work. The three angles follow a Bunge convention. During run 1, \* indicates the cycle at 425 K; Orientations differ due to the rotation induced when put in the oven.

31 These Euler angles can be used to plot pole figures of interest, such as the one displayed  
32 in the main text, or another example in Fig. S4, in the case of Run 1, cycle 2 and this work  
33 OR.

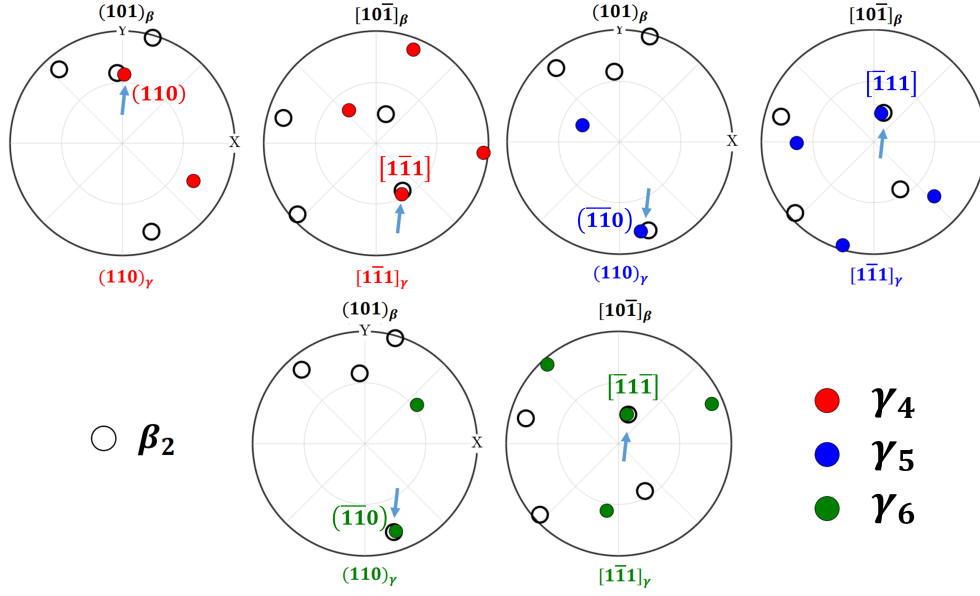


FIG. S4: Run 1, cycle 2: pole figures showing this work OR  $((101)_\beta || (110)_\gamma$  and  $[10\bar{1}]_\beta || [1\bar{1}1]_\gamma$ ) between  $\beta_2$  (empty circle) and  $\gamma_4$  (red circles),  $\gamma_5$  (blue circles) and  $\gamma_6$  (green circles). Arrows are visual guides to highlight the coincidences. The identification of plane and direction related to the mechanism are displayed for  $\gamma$ -Sn. X (horizontal) is the compression direction.

34 **S.E. X-RAY SETUP AND RELEVANT ACQUISITION PARAMETERS**

35 Experimental conditions for the 2 static experiments are summarized in Table S4, together  
 36 with the relevant acquisition parameters used for multiexposure.

Run	sample form	P range (GPa)	$\theta_{max}$	$\theta_{step}$	Number of cycles	P gauge
1	powder grains	1-12	10°	1°	3	Au [35]
2	annealed foil	5-15	24°	1°	4.5	NaCl [36]

TABLE S4: Experimental conditions of Runs 1 and 2. One cycle corresponds to one experimental path in pressure that induced  $\beta$ -Sn $\rightarrow$  $\gamma$ -Sn $\rightarrow$  $\beta$ -Sn transformations.  $\theta_{max}$  is the maximum rotation angle of the diamond anvil cell around a vertical axis used for the XRD data collection, and  $\theta_{step}$  is its step used for the multiexposures.

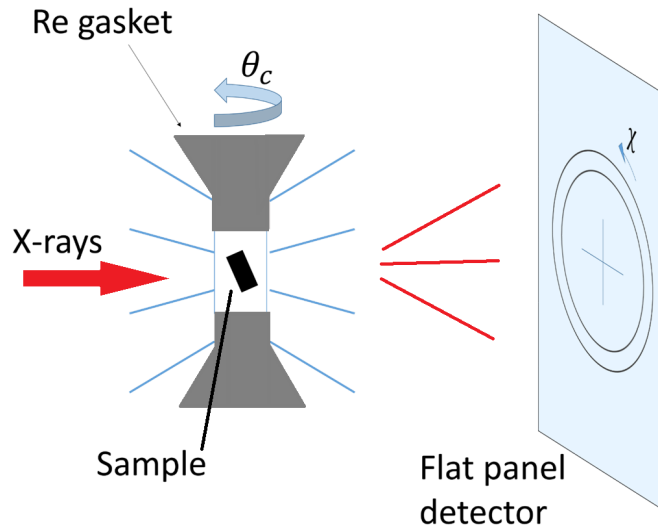


FIG. S5: Schematic representation of the X-ray diffraction setup used during the experiments.

37 **S.F. VARIANTS CREATED BY THE PROPOSED MECHANISM**

Planes	Directions	Variant name	Planes	Directions	Variant name
$(101)_\beta    (110)_\gamma$	$[\bar{1}01]_\beta    [\bar{1}11]_\gamma$	V.1	$(0\bar{1}1)_\beta    (110)_\gamma$	$[011]_\beta    [\bar{1}11]_\gamma$	V.5
	$[\bar{1}01]_\beta    [1\bar{1}1]_\gamma$	V.2		$[011]_\beta    [1\bar{1}1]_\gamma$	V.6
$(\bar{1}01)_\beta    (110)_\gamma$	$[101]_\beta    [\bar{1}11]_\gamma$	V.3	$(011)_\beta    (110)_\gamma$	$[0\bar{1}1]_\beta    [\bar{1}11]_\gamma$	V.7
	$[101]_\beta    [1\bar{1}1]_\gamma$	V.4		$[0\bar{1}1]_\beta    [1\bar{1}1]_\gamma$	V.8

TABLE S5: The eight possible variant of  $\gamma_{Sn}$  that can be produced starting from a single orientation of  $\beta_{Sn}$ , using the mechanism of this work.

38 **S.G. COMPARISON BETWEEN MECHANISMS**

39 Table S6 displays misorientation angles (in degrees) between measured orientations and  
40 theoretical orientations for runs 1 and 2, respectively. Theoretical orientations are associated  
41 with the transformation sequences given in the first two lines for several transitions reported  
42 in this work. These values were obtained using Vigilano software [52].

	TW	$(101)_\beta+$ $(101)_\beta+K$	$(301)_\beta+$ $(301)_\beta+K$	$(101)_\beta+K$ $+(112)_\gamma$	$(301)_\beta+$ $K+(112)_\gamma$	$K+(112)_\gamma$ $+(112)_\gamma$	$K+(101)_\gamma$ $+(101)_\gamma$	$(301)_\beta+K$ $+(101)_\gamma$	$(101)_\beta+K$ $+(101)_\gamma$	K $+(101)_\gamma$	K $+(112)_\gamma$	$(301)_\beta$ $+K$	$(101)_\beta$ $+K$	K
$\beta_2 \leftarrow \gamma_2$	2.19	2.18	4.99	5.94	6.16	6.68	10.81	14.98	15.82	12.88	24.53	24.95	26.16	39
$\beta_2 \leftarrow \gamma_4$	2.4	2.23	3.91	4.38	4.87	5.57	10	16.05	16.94	12.51	24.18	24.67	26.03	40.24
$\beta_2 \leftarrow \gamma_5$	2.46	3.3	4.58	5.98	5.7	6.05	9.84	15.94	16.55	12.36	24.5	25	26.38	40.46
$\beta_2 \leftarrow \gamma_6$	0.79	2.19	2.76	4.3	3.95	4.47	11.5	14.55	15.34	14.14	22.66	23.13	24.48	40.49
$\beta_A \rightarrow \gamma_A$	1.91	3.81	3.97	6.24	5.2	5.25	11.32	14.67	15.1	13.99	23.1	23.6	24.99	40.93
$\beta_A \rightarrow \gamma_B$	1.26	3.26	2.43	4.85	3.68	3.86	12.96	13.23	13.89	15.69	21.23	21.7	23.02	40.82
$\beta_B \leftarrow \gamma_A$	5.33	6.73	4.34	6.29	4.64	4.41	9.73	18.08	18.64	13.51	22.02	22.66	24.34	44.66
$\beta_B \rightarrow \gamma_{2A}$	10.92	9.18	13.35	12.46	14.23	15.10	16.69	15.68	14.61	16.22	24.26	23.74	22.72	29.99
$\beta_B \rightarrow \gamma_{2B}$	1.22	1.17	3.65	4.51	4.77	5.41	12.34	13.67	14.68	14.61	22.74	23.14	24.31	39.2
$\beta_C \leftarrow \gamma_{2A}$	6.55	8.09	4.88	6.98	4.82	4.24	10.93	18.38	18.48	14.71	20.36	21.02	22.79	45.0
$\beta_C \leftarrow \gamma_{2B}$	6.69	8.61	6.25	9.18	6.74	5.88	17.42	10.82	10.48	20.47	17.2	17.68	19.10	40.79
$\beta_C \rightarrow \gamma_E$	1.4	1.65	2.76	3.63	3.81	4.54	12.46	13.82	14.84	14.95	22.09	22.52	23.77	39.89
$\beta_C \rightarrow \gamma_F$	1.24	1.86	3.82	4.98	5	5.53	11.06	14.79	15.62	13.44	23.59	24.04	25.32	39.78
$\beta_C \rightarrow \gamma_G$	3.07	4.18	3.76	5.61	4.67	4.82	15.1	11.1	11.96	17.63	19.87	20.24	21.36	39.95
$\beta_C \rightarrow \gamma_H$	2.81	4.27	3.26	5.29	4.21	4.36	10.1	16.25	16.72	13.24	23.22	23.81	25.37	42.23

10

TABLE S6: Misorientation angles (in degrees) between measured orientations and theoretical orientations associated with the transformation sequences given in the first two lines (the “+” symbol meaning a chaining of transformations within the sequence) for several transitions reported in this work. TW: transformation mechanism proposed in this work that produces  $(101)_\beta || (110)_\gamma$  and  $[10\bar{1}]_\beta || [1\bar{1}1]_\gamma$ . OR. K: Kitzke mechanism. The twins are defined in Table S1.

43 **S.H. COMPUTATION OF THE TRANSFORMATION STRAIN**

44 The transformation strain tensor explaining TW OR is computed in two steps. First, a  
 45 shearing  $F_1$  is evaluated so that atomic distances in  $(101)_\beta$  planes after shuffle match those  
 46 in  $\gamma$ -Sn. In particular, this plane contains the  $a$  axis of  $\gamma$ -Sn and a diagonal between  $a$  and  $b$   
 47 axes, denoted in the following as ' $a/b$  diagonal'. Second, a second transformation  $F_2$ , leaving  
 48  $(101)_\beta$  planes invariant, needs to restore normal distances according to  $\gamma$ -Sn dimensions  
 49 and enforce the orthogonality between the two  $a/b$  diagonals. The total transformation is  
 50 obtained by combining these two strains

51 **Step 1**

52 Let us consider, in the  $\beta$ -Sn cell after the shuffle described in Figure 4, the vectors  $v_1 =$   
 53  $[a_\beta, a_\beta, c_\beta]/2$  and  $v_2 = [-a_\beta, a_\beta, c_\beta]/2$ . They must become a vertical axis and an  $a/b$  diagonal  
 54 of the  $\gamma$ -Sn cell after transformation, respectively. Let us work in the plane  $(\tilde{X}, \tilde{Y})$  where  
 55  $X = [0, a_\beta, 0]$ ,  $Y = [a_\beta, 0, -c_\beta]$ , and the tilde designates the normalization operator. In this  
 56 basis, the transformation stretch  $U$  to be determined must verify:

$$\left\{ \begin{array}{l} U \cdot \begin{pmatrix} 0 \\ \sqrt{a_\beta^2 + c_\beta^2} \end{pmatrix} = \begin{pmatrix} 0 \\ \sqrt{2a_\gamma^2 + c_\gamma^2} \end{pmatrix} \\ U \cdot \begin{pmatrix} \frac{a_\beta}{2} \\ \frac{\sqrt{a_\beta^2 + c_\beta^2}}{2} \end{pmatrix} = \begin{pmatrix} \frac{\sqrt{2}a_\gamma c_\gamma}{\sqrt{2a_\gamma^2 + c_\gamma^2}} \\ \frac{2a_\gamma^2}{\sqrt{2a_\gamma^2 + c_\gamma^2}} \end{pmatrix} \end{array} \right. \quad (4)$$

57 After computation, one may obtain:

$$U = \begin{pmatrix} \frac{2\sqrt{2}a_\gamma c_\gamma}{a_\beta \sqrt{2a_\gamma^2 + c_\gamma^2}} & 0 \\ \frac{2a_\gamma^2 - c_\gamma^2}{a_\beta \sqrt{2a_\gamma^2 + c_\gamma^2}} & \frac{\sqrt{2a_\gamma^2 + c_\gamma^2}}{\sqrt{a_\beta^2 + c_\beta^2}} \end{pmatrix} \quad (5)$$

58 The tensor  $F_1$  in equation 7 is then obtained as:

$$F_1 = Q \cdot \begin{pmatrix} U_{11} & U_{12} & 0 \\ U_{21} & U_{22} & 0 \\ 0 & 0 & 1 \end{pmatrix} \cdot Q^T, \quad (6)$$

59 where  $T$  is the transpose operator and  $Q = [\tilde{X}, \tilde{Y}, \tilde{X} \wedge \tilde{Y}]$ .

60 For the following values:  $a_\beta = 5.58 \text{ \AA}$  and  $c_\beta = 3.03 \text{ \AA}$  and  $a_\gamma = 3.694 \text{ \AA}$  and  $c_\gamma = 3.37$   
 61  $\text{ \AA}$ , the shear strain is:

$$F_1 = \begin{bmatrix} 0.984 & 0.404 & 0.009 \\ 0. & 1.015 & 0. \\ 0.009 & -0.219 & 0.995 \end{bmatrix}. \quad (7)$$

## 62 Step 2

63 Let us now consider  $v_3 = [-a_\beta, a_\beta, -3c_\beta]/2$ . This vector becomes the other  $a/b$  diagonal  
 64 of the  $\gamma$ -Sn cell after transformation. It will then be orthogonal to the transformed  $(101)_\beta$   
 65 plane. Let  $n$  be the normal to this plane.  $v_3$  is decomposed as follows:  $v_3 = (v_3 \cdot n)n + d \cdot m$   
 66 with  $m$  a normalized vector. The tensor  $F_2$  is then obtained as:

$$F_2 = I + \frac{\sqrt{2}a_\gamma - v_3 \cdot n}{v_3 \cdot n} n \otimes n + \frac{d}{v_3 \cdot n} m \otimes n, \quad (8)$$

67 with  $I$  the identity of second-order tensors.

68 After calculation, its components are such that:

$$F_2 = \begin{bmatrix} 1.075 & 0. & 0.138 \\ 0.254 & 1. & 0.467 \\ -0.051 & 0. & 0.906 \end{bmatrix}. \quad (9)$$

69 The total transformation is obtained by combining these two strains:

$$F = F_2 \cdot F_1 = \begin{bmatrix} 1.06 & 0.40 & 0.15 \\ 0.25 & 1.02 & 0.47 \\ -0.04 & -0.22 & 0.90 \end{bmatrix}. \quad (10)$$

70 Once this transformation strain is known, it can be applied to a group of shuffled  $\beta$ -Sn cells  
 71 to find three vectors with norms  $a_\gamma$ ,  $a_\gamma$  and  $c_\gamma$  forming a direct orthonormal basis. The  
 72 corresponding rotation matrix from  $\beta$ -Sn to  $\gamma$ -Sn lattice is:

$$\mathcal{R} = \begin{bmatrix} -0.18 & 0.86 & -0.48 \\ -0.38 & 0.38 & 0.84 \\ 0.90 & 0.34 & 0.26 \end{bmatrix}. \quad (11)$$

73 It can be easily verified that the rotation  $\mathcal{R}$  permits verifying the observed OR:  $(101)_\beta || (110)_\gamma$   
 74 and  $[10\bar{1}]_\beta || [1\bar{1}1]_\gamma$ .